Mechanism for nematic superconductivity in FeSe

Jian-Huang She[1], Michael J. Lawler[2,1,3], and Eun-Ah Kim[1,3]
[1]*Department of Physics, Cornell University, Ithaca, NY 14853, USA*
[2]*Department of physics, Binghamton University, Vestal, NY 13850, USA*
[3]*Kavli Institute for Theoretical Physics, Kohn Hall, University of California Santa Barbara, CA 93106-4030, USA*
(Dated: January 27, 2017 [file: FeSe-arxiv])

Despite its seemingly simple composition and structure, the pairing mechanism of FeSe remains an open problem due to several striking phenomena. Among them are nematic order without magnetic order, nodeless gap and unusual inelastic neutron spectra with a broad continuum, and gap anisotropy consistent with orbital selection of unknown origin. Here we propose a microscopic description of a nematic quantum paramagnet that reproduces key features of neutron spectra averaged over nematic domains. We then study how the spin fluctuations of the local moments lead to pairing within a spin-fermion model. We find the resulting superconducting order parameter to be nodeless $s \pm d$-wave within each domain. Further we show that orbital selective Hund's coupling can readily capture observed gap anisotropy. Our prediction for the inelastic neutron spectra within a single nematic domain calls for inelastic neutron scattering in a detwinned sample.

The pairing mechanism and gap symmetry of bulk[1–3] and single layer[4] FeSe is an open issue that inhibits an overarching understanding of iron-based superconductors. Although a spin-fluctuation mediated pairing scenario is a broadly accepted mechanism in iron-based superconductors,[5,6] much debate continues to focused around two distinct perspectives: weak coupling and strong coupling. Weak coupling approaches are sensitive to the band structure and generally predict dominantly $(\pi, 0)$, $(0, \pi)$ spin density wave fluctuations that couple hole pockets to electron pockets in all Fe-pnictides as well as in bulk FeSe.[7] Strong coupling approaches take strong electron-electron correlations to generate quasi-localized moments that would interact with itinerant carriers.

FeSe presents new challenges to both perspectives, including explaining its nematic order[8](see Fig 1(a)), its absence of magnetism, its gapped but active spin fluctuations at (π, π) in addition to $(\pi, 0)$[9] and its nodeless superconducting gap. There have been much efforts to address these issues. RPA based weak-coupling approaches focused on looking into implications of assumed nematic order.[10,11] Renormalization group approaches found the same effective interaction promoting spin density wave to be also promoting orbital order.[7,12,13] Approaches focusing on sizable local moments[14] led to proposals of quadrupolar order accompanying nematic order[15,16] and the proposal of an AKLT-like quantum paramagnetic nematic state.[17] Nevertheless, strikingly unique inelastic neutron spectra (INS) of FeSe evade the approaches so far one way or another. Specifically, the spin gap, the coexistence of Neel fluctuation at (π, π) and stripe fluctuation at $(\pi, 0)$, and the striking continuum between two bands over an energy range of ≈ 200meV[9] are all beyond dispersing one-magnon band picture.

The absence of the stripe order common in Fe-based superconductors was attributed to the notion of frustration.[17,18] Specifically, first principles calculations by Glasbrenner et al. [18] showed that various ordering possibilities are in close energetic competition over a wide range of model parameters for FeSe. Wang et al. [17] proposed a strong-coupling mechanism for nematic order based on this frustration: local moments form a quasi-one dimensional AKLT-like state that is a quantum paramagnetic (QPM) that naturally breaks C_4 symmetry of the square lattice into C_2. Indeed FeSe is close to a classic situation for frustrated magnets in the much studied J_1-J_2 model[19,20](see Fig. 1(b)), with $J_2 \approx J_1/2$. It has been noted from DMRG studies that J_1-J_2 model has an intermediate paramagnetic phase between stripe order and Neel order state.[21,22] A recent DMRG study of J_1-J_2-K_1-K_2 spin model found a nematic QPM state between the Neel and stripe ordered states.[23] Nevertheless INS spectra of FeSe with low energy weights at $(\pi, 0)$, $(0, \pi)$ and at (π, π) that merge around (π, π) at higher

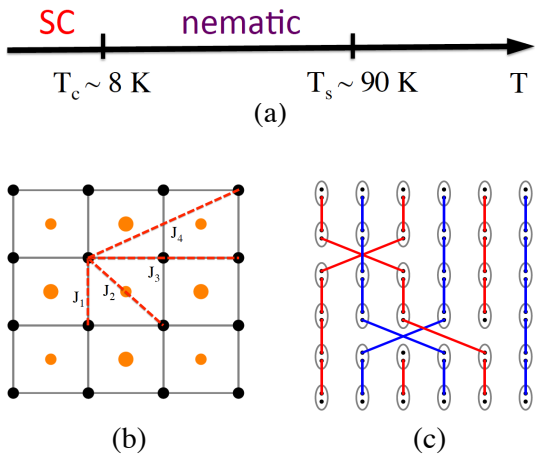

FIG. 1: (Color online) (a) Phase diagram of FeSe. (b) Lattice structure of FeSe. The black dots represent Fe atoms, and the orange dots represent Se atoms above and below the Fe plane. J_{1-4} denote the exchange couplings. (c) The nematic quantum paramagnetic state of FeSe. Each ellipse with two dots represents an $S = 1$ spin. The red and blue lines represent bonds connecting odd and even columns of spins.

energies (see Fig. 2) do not fit into any of the previously considered quantum paramagnetic states. In this letter we propose a microscopic description of the frustration driven nematic QPM state that captures the observed INS. We then investigate the implication of dramatically anisotropic spin-fluctuation spectra of the proposed state on the nature of superconductivity.

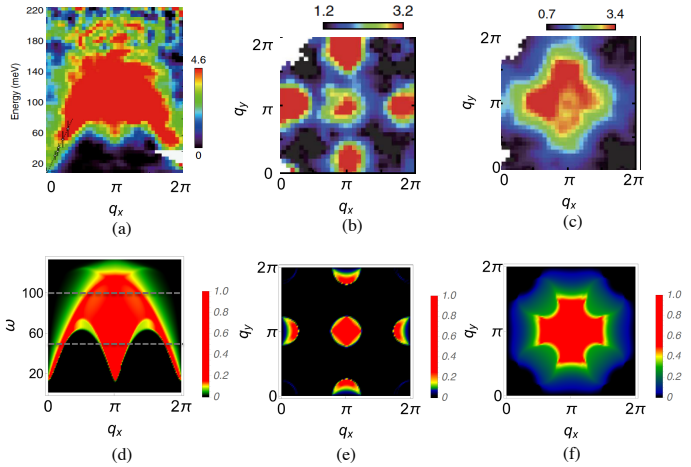

FIG. 2: (Color online) (a, b, c): Neutron scattering results for the dynamic spin structure factor $\mathcal{S}(q_x, q_y, \omega)$ at $q_y = \pi$ (a), $\omega = 50, 100$ meV (b, c).[9] (d, e, f): The corresponding results from theoretical calculation using SBMFT summed over two nematic domains.

In FeSe, there is evidence that local moments with spin close to one[14] coexist with itinerant carriers of all three t_{2g} orbitals.[24–26] In order to capture the dual character[27] of local moments and itinerant carriers simultaneously we turn to a spin-fermion model[28–33]: $\mathcal{H} = \mathcal{H}_c + \mathcal{H}_S + \mathcal{H}_{\rm int}$, where $\mathcal{H}_c$ and $\mathcal{H}_S$ describe the itinerant carriers and local moments respectively that are coupled through $\mathcal{H}_{\rm int}$. For the spin model we consider

$$\mathcal{H}_S = \sum_{ij} J_{ij} \boldsymbol{S}_i \cdot \boldsymbol{S}_j, \tag{1}$$

with exchange interaction J_{ij} on a square lattice (Fig.1b). The two dominant interactions for the Fe-spins are the nearest neighbor J_1 and the next nearest neighbor J_2 exchange interactions as in other Fe-based superconductors,[34,35] except that FeSe is in a more frustrated regime.[18]

Since the J_1-J_2 spin model is a prototype of frustrated magnetic systems, the model has been extensively studied using various methods (see[19–22]). In particular, at $J_2 = J_1/2$, the spin Hamiltonian can be written in the elegant form $\mathcal{H}_S = J_2 \sum (\boldsymbol{S}_1 + \boldsymbol{S}_2 + \boldsymbol{S}_3 + \boldsymbol{S}_4)^2$ up to a constant, where $\boldsymbol{S}_{1-4}$ are the four spins on each plaquette and the summation is over all plaquettes.[20] The ground states thus have the special property that the four spins on a plaquette sum to zero, i.e. $\boldsymbol{S}_1 + \boldsymbol{S}_2 + \boldsymbol{S}_3 + \boldsymbol{S}_4 = 0$. However as a highly frustrated model, the precise phase diagram of J_1-J_2 spin model is still elusive and there is no method to study dynamics microscopically. Hence we take a phenomenological approach guided by (1) the observed inelastic neutron spectrum,[9] and (2) the classical condition of $\boldsymbol{S}_1 + \boldsymbol{S}_2 + \boldsymbol{S}_3 + \boldsymbol{S}_4 = 0$ on a plaquette.

A prominent feature of the INS data[9] is its broad continuum of spectral weight (Fig.2a) without any one-magnon branch. Intriguingly such a continuum is expected in a quantum spin liquid with deconfined spinons in two-dimension in an insulating magnetic system.[36] In fact, the shape of the upper and lower bounds in Fig.2 resemble a 1d-like spinon dispersions: $\omega \sim \sin k_x$[37–39] except for the low energy gap in the spectra. However in a spin 1 systems on a square lattice, spinons have most often been found to be confined to form AKLT chains once fluctuations are taken into account. AKLT chains have a one-magnon branch that merges into a two-magnon continuum in parts of the Brillouin zone[40] (see also Supplemental Material SM1). On the one hand the experiment does not find any one-magnon branch, on the other hand the existence of itinerant degrees of freedom in FeSe complicates the issue beyond the reach of any available exact statements. Short of a better approach, we use Schwinger boson mean field theory (SBMFT)[41] as a calculational tool to describe the observed continuum. Not only the SBMFT formulation was useful for early works on the subject[42,43] but it offers a handle for modelling the dynamic structure factor guiding our ansatz. Although fluctuations around mean-field will confine the spinons to form a one-magnon branch in parts of the brilloin zone in a pure spin model, it is to be expected that the continuum may be still reasonably captured by the spinons. Indeed numerics show[40] the continuum in the spin-gapped AKLT state in the bilinear-biquadratic chain gradually approaches the spinon description known to exist at a phase boundary.

Another unusual feature of the neutron spectrum[9] is the simultaneous presence of both (π, π) spin fluctuations and $(\pi, 0)$, $(0, \pi)$ spin fluctuations (see Fig.2b). The (π, π) spin fluctuations are anticipated upon melting a Neel ordered ground state. On the other hand, the $(\pi, 0)/(0, \pi)$ spin fluctuations are anticipated upon melting a stripe oriented along x or y directions respectively. If we assume that apparent C_4 symmetric INS momentum distribution is a result of averaging over domains with weights focused at (π, π) and $(\pi, 0)$ or at (π, π) and $(0, \pi)$ (This is indeed consistent with the observed cross-shaped spectrum around (π, π) (see Fig.2c): otherwise the spectrum should be more rounded.), the INS spectra invites us to postulate a QPM state in which both orders are quantum melted. In particular we consider quantum melting the classical spin configurations

$$\boldsymbol{S}_{\boldsymbol{r}} = \frac{1}{2}\left[(\boldsymbol{n}_1 + \boldsymbol{n}_2)\cos(\boldsymbol{q}_1 \cdot \boldsymbol{r}) + (\boldsymbol{n}_1 - \boldsymbol{n}_2)\cos(\boldsymbol{q}_2 \cdot \boldsymbol{r})\right], \tag{2}$$

with the ordering wavevectors $\boldsymbol{q}_1 = (\pi, 0)/(0, \pi)$ respectively for the two nematic domains, $\boldsymbol{q}_2 = (\pi, \pi)$, and the spin space unit vectors $\boldsymbol{n}_{1,2}$. Such a state indeed obeys

the condition $\boldsymbol{S}_1 + \boldsymbol{S}_2 + \boldsymbol{S}_3 + \boldsymbol{S}_4 = 0$ on a plaquette, characteristic of critical spin states at $J_2 = J_1/2$.[20]

For spin 1, nematic QPMs overwhelm the phase diagram in early SBMFT model calculations through the formation of an array of 1D AKLT chains rather than a dimerized valence bond crystals.[43,44] However none of the known nematic QPMs states (see e.g.[43,44]) captures the salient features of the observed neutron spectrum,[9] specifically the simultaneous presence of both (π,π) and $(\pi,0)$, $(0,\pi)$ spin fluctuations. We will seek a new state that is (1) a 2d generalization of AKLT chains and (2) the quantum melted counterpart of the classical spin configuration Eq.(2). In Schwinger boson representation, each spin $\boldsymbol{S}_i$ is represented by two bosonic operators $b_{i\sigma}$, $\sigma = \uparrow,\downarrow$ and the constraint $\sum_\sigma b^\dagger_{i\sigma} b_{i\sigma} = 2S$. The spin operator is then $\boldsymbol{S}_i = \frac{1}{2}\sum_{\sigma\sigma'} b^\dagger_{i\sigma}\boldsymbol{\sigma}_{\sigma\sigma'} b_{i\sigma'}$, with $\boldsymbol{\sigma}$ the Pauli matrices. We can then expand $H_{ij} \equiv J_{ij}\boldsymbol{S}_i \cdot \boldsymbol{S}_j$ in terms of the spin singlet operator $A^\dagger_{ij} = b^\dagger_{i\uparrow} b^\dagger_{j\downarrow} - b^\dagger_{i\downarrow} b^\dagger_{j\uparrow}$ to obtain $H_{ij} = -J_{ij}\frac{1}{2}A^\dagger_{ij}A_{ij} + S^2$. We then mean-field decompose H_{ij} with the ansatz that sets $\langle A_{\boldsymbol{r},\boldsymbol{r}\pm\hat{y}}\rangle \neq 0$ and $\langle A_{\boldsymbol{r},\boldsymbol{r}\pm 2\hat{x}\pm\hat{y}}\rangle \neq 0$ up to fourth nearest neighbors, with $\langle A_{\boldsymbol{r},\boldsymbol{r}'}\rangle = 0$ for all other bonds $(\boldsymbol{r},\boldsymbol{r}')$ (see Fig.3). Such an ansatz state can be understood as a result of the competition between Neel and stripe states: we drop the bonds that are favored by only one of the two states, and keep only those favored by both states. In essence, this state is the coupled AKLT chain state of Ref.17 with additional J_4 bonds weakly connecting every other chain (see Fig.1c).

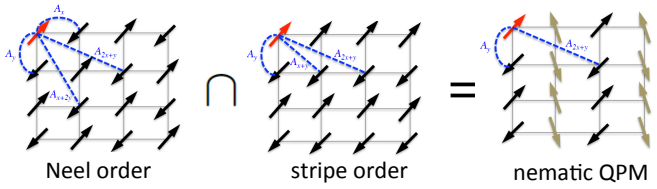

FIG. 3: (Color online) A simple nematic QPM ansatz near $J_2 = J_1/2$. Consider AFM bonds connecting the red spin with other spins. In our ansatz the bonds with nonzero expectation values are chosen to be those bonds that have nonzero expectation values in both the Neel and stripe ordered phases ($\cap$: set intersection).

We can then obtain from the SBMFT the dynamic spin structure factor $\mathcal{S}_{\boldsymbol{q}\omega} \equiv \mathrm{Im}\langle S^z(\boldsymbol{q},\omega)S^z(-\boldsymbol{q},\omega)\rangle$ associated with our ansatz. At $T = 0$, it is of the form[45]

$$\mathcal{S}_{\boldsymbol{q},\omega} \sim \sum_{\boldsymbol{k}} \left\{\cosh\left[2\left(\theta_{\boldsymbol{k}} + \theta_{\boldsymbol{k}+\tilde{\boldsymbol{q}}}\right)\right] - 1\right\} \delta\left(\omega_{\boldsymbol{k}} + \omega_{\boldsymbol{k}+\tilde{\boldsymbol{q}}} - |\omega|\right), \tag{3}$$

where $\theta_{\boldsymbol{k}}$ is the angle in the Bogoliubov transformation of SBMFT (see SM2 for explicit expression), and $\tilde{\boldsymbol{q}} = \boldsymbol{q} - (\pi,\pi)$ arises because of a standard unitary transformation we carried out on the B sublattice for simplicity. The results summing over two nematic domains are plotted in Fig. 2(d-f). They capture the basic features of the neutron spectra: (1) The spectrum is gapped (Fig. 2d), as a result of the absence of long range magnetic ordering. (2) Both (π,π) and $(\pi,0)/(0,\pi)$ spin fluctuations are present (Fig. 2d, e). This can be simply understood from the corresponding classical spin configuration Eq.(2), for which the elastic spectrum $S_{\boldsymbol{q}}S_{-\boldsymbol{q}}$ consists of two sharp peaks at (π,π) and $(\pi,0)/(0,\pi)$. (3) The spectrum displays the novel feature of continuum with the bounds exhibiting one-dimensional dispersion (Fig. 2d).

A sharp prediction of our model is the dramatic suppression of spectral weight around $(q_x,0)$ in a detwinned sample ($(0,q_y)$ for the other domain). This means at low energies there are weights at say (π,π) and $(\pi,0)$, but not at $(0,\pi)$. By contrast, in an orbital order driven picture for nematic ordering, there is only a weak anisotropy in the spin-structure factor with the spectral weight at (π,π), $(0,\pi)$ and $(\pi,0)$ of roughly the same magnitude even in a single nematic domain.[10,11] Such a distinction has profound implications for pairing. When the degree of anisotropy in the momentum distribution of the spin spectra is mild, pairing interactions with different $\boldsymbol{q}$-wavevectors compete, leading to nodes.[10,11] On the other hand, the strong anisotropy in the spectral weight distribution in our SBMFT ansatz quenches such competition removing any need for a superconducting gap node.

We now turn to the itinerant degrees of freedom to study nematicity and superconductivity. Their kinetic energy is given by a tight-binding model:

$$\mathcal{H}_c = \sum_{\boldsymbol{k},\alpha\beta,\nu} \epsilon^{\mu\nu}_{\alpha\beta}(\boldsymbol{k}) c^\dagger_{\alpha\mu}(\boldsymbol{k}) c_{\beta\nu}(\boldsymbol{k}), \tag{4}$$

where $c^\dagger_{\alpha\mu}(\boldsymbol{k})$ creates an itinerant electron with momentum $\boldsymbol{k}$, spin μ and orbital index α. What matters for pairing in the itinerant part are the low energy electronic states around the Fermi surface. The Fermi surface of FeSe consists of two electron pockets around the M points and one hole pocket around the Γ point.[24–26] Following,[6,46] we take a phenomenological approach to expand the dispersion $\epsilon^{\mu\nu}_{\alpha\beta}(\boldsymbol{k})$ around the Fermi surface. It is known experimentally that the spectral weight of the low energy states are predominantly from d_{yz} and d_{zx} around the Γ point, from d_{yz} and d_{xy} around $(\pi,0)$, from d_{zx} and d_{xy} around $(0,\pi)$. We consider the corresponding intra- and inter-orbital hopping terms. Furthermore we include on-site nematicity and spin-orbit coupling to produce the band splitting that gives rise to a single hole pocket around Γ. The resulting Fermi surface is shown in Fig.4a, see SM3 for explicit parameters.

The itinerant electrons couple to the local moments via the ferromagnetic Hund's coupling[29]:

$$\mathcal{H}_{\mathrm{int}} = -\sum_{i,\alpha,\mu\nu} J_\alpha \boldsymbol{S}_i \cdot c^\dagger_{i\alpha\mu}\boldsymbol{\sigma}_{\mu\nu} c_{i\alpha\nu}, \tag{5}$$

where $\boldsymbol{\sigma}$ represents the vector of Pauli matrices, and $J_\alpha > 0$ denote the Hund's couplings. Since the Hund's

couplings are determined by the overlap of the corresponding wavefunctions, they are generally different for different orbitals.

With such couplings, the proposed nematic QPM state induces nematicity in the charge sector. We illustrate the basic picture here using a simplified model. For instance non-zero $\langle A_{\boldsymbol{r},\boldsymbol{r}\pm\hat{y}}\rangle$ in the nematic QPM state generates an interaction among conduction electrons along the y-direction, which drives bond-centered nematic order with $\varphi_c \equiv \langle c^\dagger_{\boldsymbol{r}+\hat{x},\alpha} c_{\boldsymbol{r},\alpha} - c^\dagger_{\boldsymbol{r}+\hat{y},\alpha} c_{\boldsymbol{r},\alpha}\rangle \neq 0$ below the temperature at which the nematic QPM develops. The observed nematic transition at $T_s \sim 90K$[8] is consistent with this picture. Furthermore, φ_c linearly couples to $\varphi_o \equiv \frac{n_{zx}-n_{yz}}{n_{zx}+n_{yz}}$, where $n_{zx,yz}$ denote occupation of zx and yz orbitals, and $\varphi_s \equiv M_x^2 - M_y^2$, where $\boldsymbol{M}$ represents the magnetic moment. These different measures of nematicity are consistent with orbital imbalance observed in ARPES[24–26] ($\varphi_o \neq 0$) and the observed NMR resonance line splitting[47] ($\varphi_s \neq 0$).

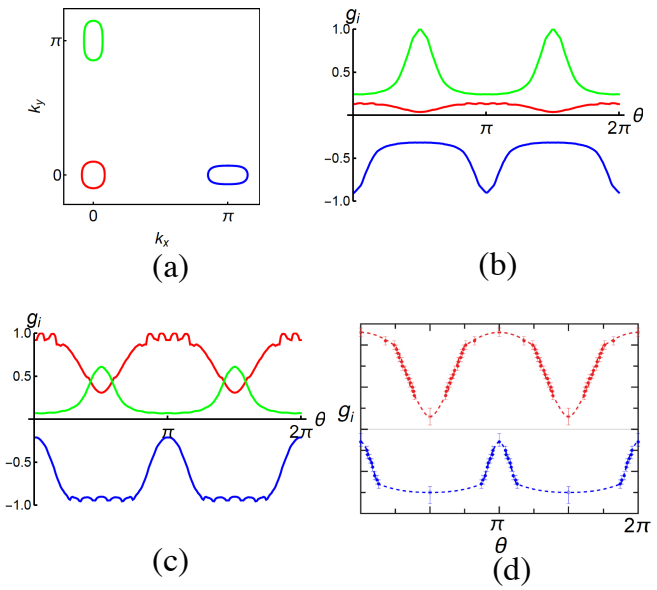

FIG. 4: (Color online) (a): The Fermi surface. (b, c): The gap symmetry function on different Fermi pockets for three-band models with $J_{yz} = J_{zx} = J_{xy} = 1$ (b) and $J_{yz} = J_{zx} = 1$, $J_{xy} = 0.4$ (c). (d): The gap function observed in the recent STM measurements.[48]

Furthermore, the nematic spin fluctuations in the proposed QPM state mediate pairing among the itinerant electrons and the resulting gap structure can be determined via standard a mean field procedure (see SM4). An immediate observation is that non-universal aspects of the gap structure such as relative gap strength of each pocket and the T_c are sensitive to strength of the Hund's couplings J's (see Fig. 4b,c). Nevertheless the gap functions resulting from our model share the following generic features: (1) The gap is generically nodeless as a result of severe anisotropy of the spin fluctuations in the nematic QPM state. In particular, the near absence of spin fluctuations around say $(0,\pi)$ for one nematic domain renders the determination of gap sign in different pockets unfrustrated. In contrast, in the itinerant model where (π,π), $(\pi,0)$ and $(0,\pi)$ spin fluctuations are close in magnitude they compete for deciding the sign structure of the gap causing nodal gap structures. (2) The gap is deeply anisotropic due to the variation of orbital content around each Fermi pocket. The resulting nodeless but very anisotropic gap structure explains the seemingly contradictory experimental results of STM,[49,50] penetration depth,[50] thermal conductivity measurements,[51] observing low energy excitations[49,50] despite the evidence of a full gap.[48,51] (3) The gap changes sign from pocket to pocket. This is consistent with the observation of sharp spin resonance in the superconducting state,[52] and is a general feature of spin-fluctuation mediated pairing. More specifically, our gap function is a combination of d-wave as induced by (π,π) spin fluctuations and $s_\pm$ as induced by $(\pi,0)$ spin fluctuations. We consider a single nematic domain, where the pairing interaction concentrates around (π, q_y). Two examples of the gap function (in arbitrary units) are shown in Fig.4b,c, where $J_{xy} = J_{yz} = J_{zx}$ and $J_{xy} = 0.4J_{yz} = 0.4J_{zx}$ respectively.

Now we turn to the question of orbital dependence of the Hund's coupling. Fig. 4b,c shows the orbital dependence of the Hund's coupling can alter the relative magnitude and anisotropy of gap functions at different Fermi pockets (while the gap is predominantly d-wave in Fig. 4b, d- and s-wave are at par in Fig. 4c). Although the spectral weight of the spin fluctuation is mostly concentrated around (π,π), itinerant electrons may not fully utilize the (π,π) fluctuation depending on the orbital dependence of the Hund's coupling. Since the Hund's coupling requires overlap of the wave-function between the conduction electrons and local moments, the observed imbalance of the weight between d_{xy} orbitals compared to d_{xz} and d_{yz} orbital imply suppression of J_{xy} compared to J_{xz} and J_{yz}. Indeed, the gap function with such orbital selective Hund's coupling shows remarkable resemblance to the gap structure observed by recent STM measurements[48] (see Fig.. 4 c,d). In Ref. Sprau et al. [48] the observed pocket specific gap anisotropy was interpreted as resulting from orbital-selective pairing of unknown microscopic origin. In our model, such orbital selective pairing arise from orbital selection in the Hund's coupling $J_{xy} < J_{yz} = J_{zx}$, reflecting much smaller weight of d_{xy} orbitals in the conduction electrons.[53] This orbital selective Hund's coupling amplify the role of $(\pi,0)$ spin fluctuation in pairing despite larger spectral weight at (π,π), which is consistent with the observation of sharp spin resonance at $(\pi,0)$.[52]

In conclusion, we propose a unified framework that explains the basic phenomenology of FeSe. (1) Spin dynamics: we propose a new nematic QPM state that explains the observed inelastic neutron spectrum[9] assuming the observed INS is averaged over domains. (2) Nematic transition: by coupling the nematic QPM to conduction

electrons to form a spin-fermion model, we obtain a nematic order parameter that explains the observed sharp nematic transition (without magnetic ordering). (3) Unconventional superconductivity: employing orbital selectivity, we obtain a fully-gapped but highly anisotropic superconducting phase that agrees with the experiments. The central assumption that neutron scattering is averaging over domain walls could be tested in a detwinned neutron experiment. Orbital selective Hund's coupling mechanisms for orbital selective pairing in bulk FeSe further offers new insight regarding higher T_c observed in mono-layer FeSe and K-doped FeSe. As we show in SM4, larger J_{xy} that enables conduction electrons to utilize (π, π) spin fluctuation with larger intensity and higher characteristic frequency leads to higher transition temperature (as high as 47K). Combined with the observation that spectral weight of the d_{xy} orbitals in the conduction electrons is much higher in the higher T_c settings of mono-layer FeSe and K-doped FeSe,[53] it is conceivable these systems make better use of already more prominent (π, π) fluctuation to achieve higher T_c. Finally, although we used SBMFT as a calculational crutch to capture the spin wave continuum, the ultimate fate of spinons in this spin-1 system coupled to itinerant electrons needs further study. Interestingly, such a state with spinons coexisting with conduction electrons would resemble the FL* state first proposed in Refs.54,55 that has recently been revisited using DMRG.[56]

Acknowledgements We thank Andrey Chubukov, J.C. Davis, Rafael Fernandes, Steve Kivelson, Igor Mazin, Andriy Nevidomskyy, Doug Scalapino, Qimiao Si, Fa Wang for discussions. E-AK and J-HS were supported by the U.S. Department of Energy, Office of Basic Energy Sciences, Division of Materials Science and Engineering under Award de-sc0010313. E-AK also acknowledges Simons Fellow in Theoretical Physics Award#392182. E-AK and MJL acknowledge hospitality of the KITP supported by Grant No. NSF PHY11-25915.

[1] J. Paglione and R. L. Greene, Nature Physics **6**, 645 (2010), 1006.4618.

[2] P. J. Hirschfeld, M. M. Korshunov, and I. I. Mazin, Reports on Progress in Physics **74**, 124508 (2011), URL http://stacks.iop.org/0034-4885/74/i=12/a=124508.

[3] Q. Si, R. Yu, and E. Abrahams, Nature Reviews Materials **1**, 16017 (2016), 1604.03566.

[4] Q.-Y. Wang, Z. Li, W.-H. Zhang, Z.-C. Zhang, J.-S. Zhang, W. Li, H. Ding, Y.-B. Ou, P. Deng, K. Chang, et al., Chinese Physics Letters **29**, 037402 (2012), 1201.5694.

[5] F. Wang and D.-H. Lee, Science **332**, 200 (2011), ISSN 0036-8075, http://science.sciencemag.org/content/332/6026/200.full.pdf, URL http://science.sciencemag.org/content/332/6026/200.

[6] R. M. Fernandes and A. V. Chubukov, ArXiv e-prints (2016), 1607.00865.

[7] A. V. Chubukov, M. Khodas, and R. M. Fernandes, Phys. Rev. X **6**, 041045 (2016), URL http://link.aps.org/doi/10.1103/PhysRevX.6.041045.

[8] T. M. McQueen, A. J. Williams, P. W. Stephens, J. Tao, Y. Zhu, V. Ksenofontov, F. Casper, C. Felser, and R. J. Cava, Phys. Rev. Lett. **103**, 057002 (2009), URL http://link.aps.org/doi/10.1103/PhysRevLett.103.057002.

[9] Q. Wang, Y. Shen, B. Pan, X. Zhang, K. Ikeuchi, K. Iida, A. D. Christianson, H. C. Walker, D. T. Adroja, M. Abdel-Hafiez, et al., Nat Commun **7** (2016), URL http://dx.doi.org/10.1038/ncomms12182.

[10] S. Mukherjee, A. Kreisel, P. J. Hirschfeld, and B. M. Andersen, Phys. Rev. Lett. **115**, 026402 (2015), URL http://link.aps.org/doi/10.1103/PhysRevLett.115.026402.

[11] A. Kreisel, S. Mukherjee, P. J. Hirschfeld, and B. M. Andersen, Phys. Rev. B **92**, 224515 (2015), URL http://link.aps.org/doi/10.1103/PhysRevB.92.224515.

[12] R.-Q. Xing, L. Classen, M. Khodas, and A. V. Chubukov, ArXiv e-prints (2016), 1611.03912.

[13] L. Classen, R.-Q. Xing, M. Khodas, and A. V. Chubukov, ArXiv e-prints (2016), 1612.08708.

[14] H. Gretarsson, A. Lupascu, J. Kim, D. Casa, T. Gog, W. Wu, S. R. Julian, Z. J. Xu, J. S. Wen, G. D. Gu, et al., Phys. Rev. B **84**, 100509 (2011), URL http://link.aps.org/doi/10.1103/PhysRevB.84.100509.

[15] R. Yu and Q. Si, Phys. Rev. Lett. **115**, 116401 (2015), URL http://link.aps.org/doi/10.1103/PhysRevLett.115.116401.

[16] Z. Wang, W.-J. Hu, and A. H. Nevidomskyy, Phys. Rev. Lett. **116**, 247203 (2016), URL http://link.aps.org/doi/10.1103/PhysRevLett.116.247203.

[17] F. Wang, S. A. Kivelson, and D.-H. Lee, Nat Phys **11**, 959 (2015), URL http://dx.doi.org/10.1038/nphys3456.

[18] J. K. Glasbrenner, I. I. Mazin, H. O. Jeschke, P. J. Hirschfeld, R. M. Fernandes, and R. Valenti, Nat Phys **11**, 953 (2015), URL http://dx.doi.org/10.1038/nphys3434.

[19] P. Chandra, P. Coleman, and A. I. Larkin, Phys. Rev. Lett. **64**, 88 (1990), URL http://link.aps.org/doi/10.1103/PhysRevLett.64.88.

[20] G. Misguich and C. Lhuillier, *Two-Dimensional Quantum Antiferromagnets* (World Scientific Publishing Co, 2004), pp. 229–306.

[21] H. C. Jiang, F. Krüger, J. E. Moore, D. N. Sheng, J. Zaanen, and Z. Y. Weng, Phys. Rev. B **79**, 174409 (2009), URL http://link.aps.org/doi/10.1103/PhysRevB.79.174409.

[22] H.-C. Jiang, H. Yao, and L. Balents, Phys. Rev. B **86**, 024424 (2012), URL http://link.aps.org/doi/10.1103/PhysRevB.86.024424.

[23] S.-S. Gong, W. Zhu, D. N. Sheng, and K. Yang, ArXiv e-prints (2016), 1606.00937.

[24] K. Nakayama, Y. Miyata, G. N. Phan, T. Sato, Y. Tanabe, T. Urata, K. Tanigaki, and T. Takahashi, Phys. Rev. Lett. **113**, 237001 (2014), URL http://link.aps.org/doi/10.1103/PhysRevLett.113.237001.

[25] M. D. Watson, T. K. Kim, A. A. Haghighirad, N. R. Davies, A. McCollam, A. Narayanan, S. F. Blake, Y. L. Chen, S. Ghannadzadeh, A. J. Schofield, et al., Phys. Rev.

B **91**, 155106 (2015), URL http://link.aps.org/doi/10.1103/PhysRevB.91.155106.

[26] Y. Suzuki, T. Shimojima, T. Sonobe, A. Nakamura, M. Sakano, H. Tsuji, J. Omachi, K. Yoshioka, M. Kuwata-Gonokami, T. Watashige, et al., Phys. Rev. B **92**, 205117 (2015), URL http://link.aps.org/doi/10.1103/PhysRevB.92.205117.

[27] S. J. Moon, J. H. Shin, D. Parker, W. S. Choi, I. I. Mazin, Y. S. Lee, J. Y. Kim, N. H. Sung, B. K. Cho, S. H. Khim, et al., Phys. Rev. B **81**, 205114 (2010), URL http://link.aps.org/doi/10.1103/PhysRevB.81.205114.

[28] S.-P. Kou, T. Li, and Z.-Y. Weng, EPL (Europhysics Letters) **88**, 17010 (2009), URL http://stacks.iop.org/0295-5075/88/i=1/a=17010.

[29] W. Lv, F. Krüger, and P. Phillips, Phys. Rev. B **82**, 045125 (2010), URL http://link.aps.org/doi/10.1103/PhysRevB.82.045125.

[30] W.-G. Yin, C.-C. Lee, and W. Ku, Phys. Rev. Lett. **105**, 107004 (2010), URL http://link.aps.org/doi/10.1103/PhysRevLett.105.107004.

[31] V. Stanev and P. B. Littlewood, Phys. Rev. B **87**, 161122 (2013), URL http://link.aps.org/doi/10.1103/PhysRevB.87.161122.

[32] S. Liang, A. Mukherjee, N. D. Patel, C. B. Bishop, E. Dagotto, and A. Moreo, Phys. Rev. B **90**, 184507 (2014), URL http://link.aps.org/doi/10.1103/PhysRevB.90.184507.

[33] D.-H. Lee, Chinese Physics B **24**, 117405 (2015), URL http://stacks.iop.org/1674-1056/24/i=11/a=117405.

[34] C. Fang, H. Yao, W.-F. Tsai, J. Hu, and S. A. Kivelson, Phys. Rev. B **77**, 224509 (2008), URL http://link.aps.org/doi/10.1103/PhysRevB.77.224509.

[35] C. Xu, M. Müller, and S. Sachdev, Phys. Rev. B **78**, 020501 (2008), URL http://link.aps.org/doi/10.1103/PhysRevB.78.020501.

[36] L. Balents, Nature **464**, 199 (2010).

[37] G. Müller, H. Thomas, H. Beck, and J. C. Bonner, Phys. Rev. B **24**, 1429 (1981), URL http://link.aps.org/doi/10.1103/PhysRevB.24.1429.

[38] B. Lake, D. A. Tennant, J.-S. Caux, T. Barthel, U. Schollwöck, S. E. Nagler, and C. D. Frost, Phys. Rev. Lett. **111**, 137205 (2013), URL http://link.aps.org/doi/10.1103/PhysRevLett.111.137205.

[39] R. Vlijm and J.-S. Caux, Journal of Statistical Mechanics: Theory and Experiment **5**, 05009 (2014), 1401.4450.

[40] A. Schmitt, K.-H. Mütter, M. Karbach, Y. Yu, and G. Müller, Phys. Rev. B **58**, 5498 (1998), URL http://link.aps.org/doi/10.1103/PhysRevB.58.5498.

[41] D. P. Arovas and A. Auerbach, Phys. Rev. B **38**, 316 (1988), URL http://link.aps.org/doi/10.1103/PhysRevB.38.316.

[42] F. D. M. Haldane, Phys. Rev. Lett. **61**, 1029 (1988), URL http://link.aps.org/doi/10.1103/PhysRevLett.61.1029.

[43] S. Sachdev and N. Read, International Journal of Modern Physics B **5**, 219 (1991), cond-mat/0402109.

[44] N. Read and S. Sachdev, Phys. Rev. B **42**, 4568 (1990), URL http://link.aps.org/doi/10.1103/PhysRevB.42.4568.

[45] A. Auerbach and D. P. Arovas, Phys. Rev. Lett. **61**, 617 (1988), URL http://link.aps.org/doi/10.1103/PhysRevLett.61.617.

[46] V. Cvetkovic and O. Vafek, Phys. Rev. B **88**, 134510 (2013), URL http://link.aps.org/doi/10.1103/PhysRevB.88.134510.

[47] S.-H. Baek, D. V. Efremov, J. M. Ok, J. S. Kim, J. van den Brink, and B. Büchner, Nat Mater **14**, 210 (2015), URL http://dx.doi.org/10.1038/nmat4138.

[48] P. O. Sprau, A. Kostin, A. Kreisel, A. E. Böhmer, V. Taufour, P. C. Canfield, S. Mukherjee, P. J. Hirschfeld, B. M. Andersen, and J. C. Séamus Davis, ArXiv e-prints (2016), 1611.02134.

[49] C.-L. Song, Y.-L. Wang, P. Cheng, Y.-P. Jiang, W. Li, T. Zhang, Z. Li, K. He, L. Wang, J.-F. Jia, et al., Science **332**, 1410 (2011), ISSN 0036-8075, http://science.sciencemag.org/content/332/6036/1410.full.pdf, URL http://science.sciencemag.org/content/332/6036/1410.

[50] S. Kasahara, T. Watashige, T. Hanaguri, Y. Kohsaka, T. Yamashita, Y. Shimoyama, Y. Mizukami, R. Endo, H. Ikeda, K. Aoyama, et al., Proceedings of the National Academy of Sciences **111**, 16309 (2014), http://www.pnas.org/content/111/46/16309.full.pdf, URL http://www.pnas.org/content/111/46/16309.abstract.

[51] P. Bourgeois-Hope, S. Chi, D. A. Bonn, R. Liang, W. N. Hardy, T. Wolf, C. Meingast, N. Doiron-Leyraud, and L. Taillefer, Phys. Rev. Lett. **117**, 097003 (2016), URL http://link.aps.org/doi/10.1103/PhysRevLett.117.097003.

[52] Q. Wang, Y. Shen, B. Pan, Y. Hao, M. Ma, F. Zhou, P. Steffens, K. Schmalzl, T. R. Forrest, M. Abdel-Hafiez, et al., Nature Materials **15**, 159 (2016), 1502.07544.

[53] M. Yi, Z.-K. Liu, Y. Zhang, R. Yu, J.-X. Zhu, J. J. Lee, R. G. Moore, F. T. Schmitt, W. Li, S. C. Riggs, et al., Nature Communications **6**, 7777 (2015), 1506.03888.

[54] T. Senthil, S. Sachdev, and M. Vojta, Phys. Rev. Lett. **90**, 216403 (2003), URL http://link.aps.org/doi/10.1103/PhysRevLett.90.216403.

[55] T. Senthil, M. Vojta, and S. Sachdev, Phys. Rev. B **69**, 035111 (2004), URL http://link.aps.org/doi/10.1103/PhysRevB.69.035111.

[56] J. Lee, S. Sachdev, and S. R. White, Phys. Rev. B **94**, 115112 (2016), URL http://link.aps.org/doi/10.1103/PhysRevB.94.115112.

[57] A. Läuchli, G. Schmid, and S. Trebst, Phys. Rev. B **74**, 144426 (2006), URL http://link.aps.org/doi/10.1103/PhysRevB.74.144426.

[58] S. R. Manmana, A. M. Läuchli, F. H. L. Essler, and F. Mila, Phys. Rev. B **83**, 184433 (2011), URL http://link.aps.org/doi/10.1103/PhysRevB.83.184433.

[59] L. A. Takhtajan, Phys. Lett. **A87**, 479 (1982).

[60] H. M. Babujian, Phys. Lett. **A90**, 479 (1982).

[61] D. A. Kirzhnits, E. G. Maksimov, and D. I. Khomskii, Journal of Low Temperature Physics **10**, 79 (1973), ISSN 1573-7357, URL http://dx.doi.org/10.1007/BF00655243.

[62] S. N. Klimin, J. Tempere, J. T. Devreese, and D. van der Marel, Phys. Rev. B **89**, 184514 (2014), URL http://link.aps.org/doi/10.1103/PhysRevB.89.184514.

[63] S. Kasahara, T. Watashige, T. Hanaguri, Y. Kohsaka, T. Yamashita, Y. Shimoyama, Y. Mizukami, R. Endo, H. Ikeda, K. Aoyama, et al., Proceedings of the National Academy of Sciences **111**, 16309 (2014), http://www.pnas.org/content/111/46/16309.full.pdf, URL http://www.pnas.org/content/111/46/16309.abstract.

[64] Y. Miyata, K. Nakayama, K. Sugawara, T. Sato, and

T. Takahashi, Nat Mater **14**, 775 (2015), URL http://dx.doi.org/10.1038/nmat4302.

[65] J. J. Lee, F. T. Schmitt, R. G. Moore, S. Johnston, Y. T. Cui, W. Li, M. Yi, Z. K. Liu, M. Hashimoto, Y. Zhang, et al., Nature **515**, 245 (2014), URL http://dx.doi.org/10.1038/nature13894.

Supplemental Material

SM1: Review of 1d $S = 1$ spin chain

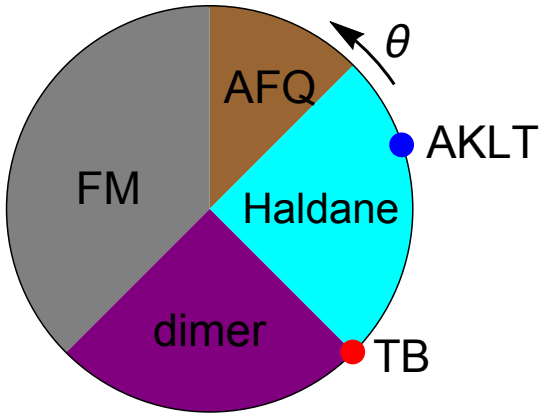

FIG. 5: (Color online) Phase diagram of 1d $S = 1$ spin chains with bilinear and biquadratic interactions.[57,58]

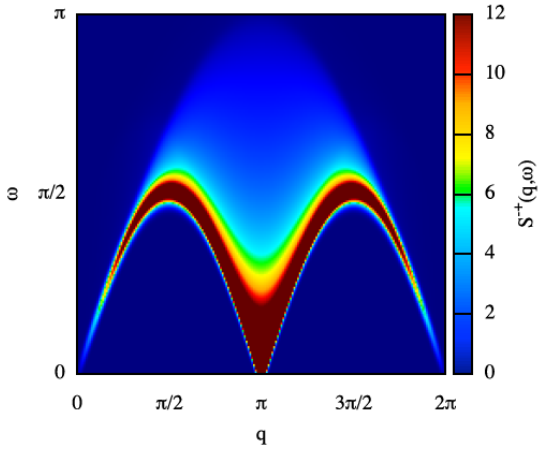

FIG. 6: (Color online) Dynamic spin structure factor of Takhtajan-Babujian chain as obtained in Bethe Ansatz.[39]

We include here a brief review of the 1d $S = 1$ spin chains with bilinear and biquadratic interactions with an emphasis on their dynamic spin spectrum. The Hamiltonian is

$$\mathcal{H}_S = J \sum_i \left[\cos\theta \left(\boldsymbol{S}_i \cdot \boldsymbol{S}_{i+1} \right) + \sin\theta \left(\boldsymbol{S}_i \cdot \boldsymbol{S}_{i+1} \right)^2 \right], \tag{6}$$

with $-\pi \leq \theta \leq \pi$. As shown in Fig.5, this model has a rich phase diagram (see[57,58] and references therein): (1) ferromagnetic phase for $-\pi < \theta < -3\pi/4$ and $\pi/2 < \theta \leq \pi$, (2) dimerized phase for $-3\pi/4 < \theta < -\pi/4$, (3) gapped and topologically ordered Haldane phase for $-\pi/4 < \theta < \pi/4$ (the AKLT state corresponds to $\theta = \arctan \frac{1}{3} \simeq 0.1024\pi$), (4) gapless phase with antiferroquadrupolar (AFQ) correlations for $\pi/4 < \theta < \pi/2$.[57] The dimerized phase and the Haldane phase are separated by a critical point, the Takhtajan-Babujian (TB) point.[59,60] At the TB point, the system possesses gapless spinon excitations. The spinon continuum is manifest in the dynamical spin structure

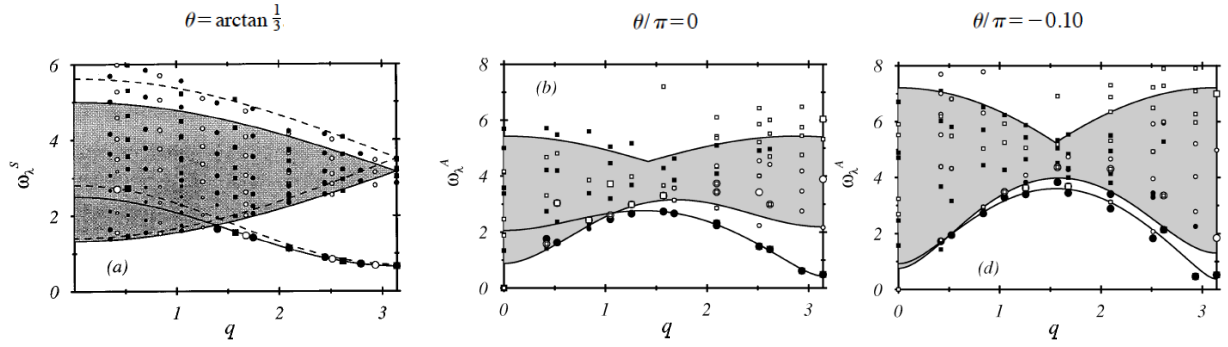

FIG. 7: (Color online) Dynamic spin structure factor of 1d $S = 1$ spin chains with the corresponding θ values as obtained in.[40]

factor (Fig.6) as obtained using algebraic Bethe ansatz-based method.[39] As one moves away from the critical point into the Haldane phase, the spinons get confined, and the elementary excitations are magnons. However one notes that the magnons are strongly interacting: in addition to the one magnon branch, the two-magnon processes have important contributions to the dynamic spin structure factor (see Fig.7).[40] As one approaches the critical point, the two-magnon excitations turn into two-sponon excitations.[40]

SM2: Schwinger boson mean field theory

We show here that our ansatz state is a self-consistent solution of the J_1-J_2-J_3-J_4 spin model (see Fig.1a of main text for definition of J's). On a bipartite lattice, it is convenient to perform a unitary transformation by defining $a_{im} \equiv b_{im}$ on A sublattice, and $a_{j\uparrow} \equiv b_{j\downarrow}$, $a_{j\downarrow} \equiv -b_{j\uparrow}$ on B sublattice. The valence bond operator is then brought to the simpler form $A^\dagger_{ij} = \sum_\sigma a^\dagger_{i\sigma} a^\dagger_{j\sigma}$. Modular a constant, the spin Hamiltonian $\mathcal{H}_S = \sum_{ij} J_{ij} \boldsymbol{S}_i \cdot \boldsymbol{S}_j$ can be written in terms of the valence bond operators as

$$\mathcal{H}_S = -\frac{1}{2} \sum_{ij} J_{ij} A^\dagger_{ij} A_{ij}. \tag{7}$$

We then apply mean field theory to the bosonic Hamiltonian.[41] Defining $Q_{ij} = J_{ij} \langle A_{ij} \rangle \equiv Q_\delta$, the quadratic part of the mean field Hamiltonian reads:

$$\mathcal{H}^{(\mathrm{MF})}_S = \lambda \sum_{i\sigma} a^\dagger_{i\sigma} a_{i\sigma} + \frac{1}{2} \sum_{i\delta\sigma} Q_\delta \left(a^\dagger_{i\sigma} a^\dagger_{i+\delta,\sigma} + a_{i\sigma} a_{i+\delta,\sigma} \right). \tag{8}$$

For a given mean field ansatz, the mean field Hamiltonian can be diagonalized by the Bogoliubov transformation

$$\alpha_{\boldsymbol{k}\sigma} = \cosh \theta_{\boldsymbol{k}} a_{\boldsymbol{k}\sigma} - \sinh \theta_{\boldsymbol{k}} a^\dagger_{-\boldsymbol{k}\sigma}, \tag{9}$$

with $\tanh(2\theta_{\boldsymbol{k}}) = -Q\gamma_{\boldsymbol{k}}/\lambda$. Here $Q\gamma_{\boldsymbol{k}}$ denotes the Fourier transform of Q_δ: $Q\gamma_{\boldsymbol{k}} = \sum_\delta e^{-i\boldsymbol{k}\cdot\boldsymbol{\delta}}$. The resulting Hamiltonian reads

$$\mathcal{H}^{(\mathrm{MF})}_S = \sum_{\boldsymbol{k}\sigma} \omega_{\boldsymbol{k}} \left(\alpha^\dagger_{\boldsymbol{k}\sigma} \alpha_{\boldsymbol{k}\sigma} + \frac{1}{2} \right), \tag{10}$$

with the dispersion $\omega_{\boldsymbol{k}} = \sqrt{\lambda^2 - (Q\gamma_{\boldsymbol{k}})^2}$. For the nematic PM state, up to fourth nearest neighbor, the nonvanishing bonds are Q_y and Q_{2x+y}, and hence

$$Q\gamma_{\boldsymbol{k}} = 2Q_y \cos k_y + 4Q_{2x+y} \cos(2k_x) \cos(k_y). \tag{11}$$

The ansatz state is basically determined by the two dimensionless parameters: Q_y/λ and Q_{2x+y}/Q_y. We have taken $Q_y/\lambda = 0.38$ and $Q_{2x+y}/Q_y = 0.15$ for the plot of spin structure factor in the main text (Fig.2).

Integrating out the bosonic fields, one obtains the free energy

$$F = \sum_\delta \frac{|Q_\delta|^2}{2J_\delta} - \frac{1}{2}(2S+1)\lambda + \frac{1}{\beta} \int \frac{d^2\boldsymbol{k}}{(2\pi)^2} \ln \left[2 \sinh \left(\frac{1}{2} \beta \omega_{\boldsymbol{k}} \right) \right], \tag{12}$$

from which follow the self-consistency equations

$$S+\frac{1}{2} = \int \frac{d^2\boldsymbol{k}}{(2\pi)^2}\frac{\lambda}{2\omega_{\boldsymbol{k}}}, \tag{13}$$

$$\frac{Q_y}{J_1} = \int \frac{d^2\boldsymbol{k}}{(2\pi)^2}\frac{Q\gamma_{\boldsymbol{k}}}{2\omega_{\boldsymbol{k}}}\cos k_y, \tag{14}$$

$$\frac{Q_{2x+y}}{J_4} = \int \frac{d^2\boldsymbol{k}}{(2\pi)^2}\frac{Q\gamma_{\boldsymbol{k}}}{2\omega_{\boldsymbol{k}}}\cos k_y\cos(2k_x), \tag{15}$$

at $T=0$. The other bonds (Q_x, Q_{x+y}, Q_{2x}, Q_{2y}, Q_{x+2y}) vanish self-consistently. More generally, taking into account further neighbor bonds, the nematic QPM phase is characterized by $\langle A_\delta\rangle \neq 0$, with

$$\boldsymbol{\delta} = 2m\boldsymbol{e}_x + (2n+1)\boldsymbol{e}_y, \tag{16}$$

in one nematic domain, where m, n are integers.

We then show that our ansatz state can indeed represent a QPM state. In SBMFT, long-range order occurs through Bose-Einstein condensation (BEC) of the Schwinger bosons, and condensation gives rise to gapless spectrum due to the resulting Goldstone mode. The QPM state corresponds to a solution of the self-consistency equations (Eqs.13-15) with gapped spectrum, where there is no condensation of Schwinger bosons. We have numerically determined the phase boundary between the nematic QPM and nematic ordered states in the parameter space expanded by S and J_4/J_1 (see Fig.8). In particular, for $S=1/2$, the nematic PM state exists in the region $J_4/J_1 < 0.07$. We note that in the recent DMRG study of J_1-J_2-K_1-K_2 spin model, a nematic QPM state has been found to be stabilized between the Neel and stripe ordered states.[23] It would be interesting to check our ansatz state is the same as their state.

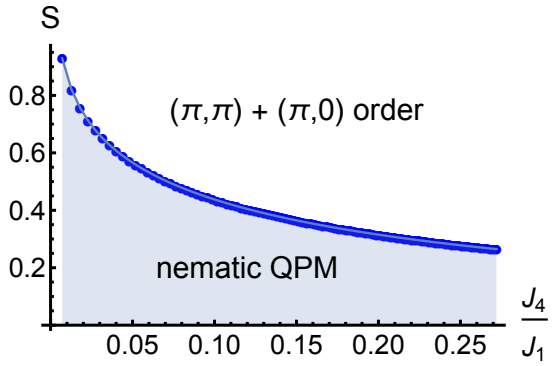

FIG. 8: (Color online) Phase diagram of our ansatz state in SBMFT.

SM3: Itinerant part: three orbital model

For the itinerant part of the system, what matters for pairing are the low energy electronic states around the Fermi pockets. We take a phenomenological approach to expand the dispersion around the Fermi pockets. Since it is known experimentally that the spectral weight of the low energy states arises mainly from d_{yz}, d_{zx}, d_{xy} orbitals, we consider a band structure involving these three orbitals. Such orbital-projected band models have been studied in.[6,46] Consider first the Fermi pocket near the Γ point, a single hole pocket has been detected, with the d_{yz} and d_{zx} orbitals dominating the spectral weight. We introduce a spinor $\psi^T_{\gamma,\boldsymbol{k}} = (c_{yz,\boldsymbol{k}\uparrow}, -c_{zx,\boldsymbol{k}\uparrow}, c_{yz,\boldsymbol{k}\downarrow}, -c_{zx,\boldsymbol{k}\downarrow})$, and the kinetic energy part of the Hamiltonian is of the form

$$\mathcal{H}_{0,\Gamma} = \sum_{\boldsymbol{k}} \psi^\dagger_{\gamma,\boldsymbol{k}} h_\Gamma(\boldsymbol{k})\psi_{\Gamma,\boldsymbol{k}}. \tag{17}$$

The Hamiltonian includes the on-site energy, intra-orbital hopping, inter-orbital hopping. To get the right orbital splitting, we include also the difference in the on-site energy for the two orbitals reflecting nematicity, and the spin-orbit coupling.[46] The result reads

$$h_\Gamma(\boldsymbol{k}) = \left(\varepsilon_\Gamma + \frac{k^2}{2m_\Gamma}\right)\tau^0\otimes\sigma^0 + \left[\delta\varepsilon_\Gamma + bk^2\cos(2\theta_k)\right]\tau^3\otimes\sigma^0 + ck^2\sin(2\theta_k)\tau^1\otimes\sigma^0 + \lambda\tau^2\otimes\sigma^3, \tag{18}$$

where τ and σ are Pauli matrices in orbital and spin space respectively, and $\boldsymbol{k} = (k_x, k_y) = k(\cos\theta_k, \sin\theta_k)$.

For the electron pocket near $(\pi, 0)$, the d_{yz} and d_{xy} orbitals dominate the spectral weight. We introduce a spinor $\psi^T_{X,\boldsymbol{k}} = (c_{yz,\boldsymbol{k}\uparrow}, c_{xy,\boldsymbol{k}\uparrow}, c_{yz,\boldsymbol{k}\downarrow}, c_{xy,\boldsymbol{k}\downarrow})$, and the kinetic energy part of the Hamiltonian is of the form

$$\mathcal{H}_{0,X} = \sum_{\boldsymbol{k}} \psi^\dagger_{X,\boldsymbol{k}} h_X(\boldsymbol{k}) \psi_{X,\boldsymbol{k}}, \tag{19}$$

with

$$h_X(\boldsymbol{k}) = \left[\varepsilon_1 + \frac{k^2}{2m_1} - a_1 k^2 \cos(2\theta_k)\right] \frac{\tau^0 + \tau^3}{2} \otimes \sigma^0 + \left[\varepsilon_3 + \frac{k^2}{2m_3} - a_3 k^2 \cos(2\theta_k)\right] \frac{\tau^0 - \tau^3}{2} \otimes \sigma^0 + 2vk \sin\theta_k \tau^2 \otimes \sigma^0. \tag{20}$$

Here $\boldsymbol{k}$ is measured from $(\pi, 0)$.

For the electron pocket near $(0, \pi)$, the d_{zx} and d_{xy} orbitals dominate the spectral weight. We introduce a spinor $\psi^T_{Y,\boldsymbol{k}} = (c_{zx,\boldsymbol{k}\uparrow}, c_{xy,\boldsymbol{k}\uparrow}, c_{zx,\boldsymbol{k}\downarrow}, c_{xy,\boldsymbol{k}\downarrow})$, and the kinetic energy part of the Hamiltonian is of the form

$$\mathcal{H}_{0,Y} = \sum_{\boldsymbol{k}} \psi^\dagger_{Y,\boldsymbol{k}} h_Y(\boldsymbol{k}) \psi_{Y,\boldsymbol{k}}, \tag{21}$$

with

$$h_Y(\boldsymbol{k}) = \left[\varepsilon_1 + \frac{k^2}{2m_1} + a_1 k^2 \cos(2\theta_k)\right] \frac{\tau^0 + \tau^3}{2} \otimes \sigma^0 + \left[\varepsilon_3 + \frac{k^2}{2m_3} + a_3 k^2 \cos(2\theta_k)\right] \frac{\tau^0 - \tau^3}{2} \otimes \sigma^0 + 2vk \cos\theta_k \tau^2 \otimes \sigma^0. \tag{22}$$

Here $\boldsymbol{k}$ is measured from $(0, \pi)$.

With a proper choice of the parameters, we can obtain a single hole pocket around Γ, a single electron pocket around $(\pi, 0)$, and a single electron pocket around $(0, \pi)$ as shown in Fig.4a of main text. The corresponding parameters are: $\varepsilon_\Gamma = 14$, $\delta\varepsilon_\Gamma = 11$, $\frac{1}{2m_\Gamma} = -350$, $b = -70$, $c = 120$, $\lambda = 9$, $\varepsilon_1 = -20$, $\varepsilon_3 = -60$ $\frac{1}{2m_1} = 75$, $\frac{1}{2m_3} = 160$, $a_1 = 100$, $a_3 = -120$, $v = -60$.

SM4: Interaction and pairing

The dynamic spin fluctuations in the QPM affect the itinerant electrons. Since the spins have a gapped spectrum, we can integrate them out to obtain an effective interaction for the itinerant electrons. The induced action reads

$$\mathcal{S}_{\rm int} = -\frac{1}{2} \int_0^\beta d\tau \sum_{\alpha,\alpha'} J_\alpha J_{\alpha'} \chi_{ij}(\tau) \boldsymbol{s}_{i\alpha}(\tau) \cdot \boldsymbol{s}_{j\alpha'}(0), \tag{23}$$

with the itinerant electron spin density $\boldsymbol{s}_{i\alpha} \equiv \sum_{\mu\nu} c^\dagger_{i\alpha\mu} \boldsymbol{\sigma}_{\mu\nu} c_{i\alpha\nu}$, and the local moment spin correlation function $\chi_{ij}(\tau) \equiv \langle T_\tau S^a_i(\tau) S^a_j(0)\rangle$. The induced interaction is highly anisotropic, and the dominant interaction term is the nearest-neighbor interaction (say along the y-direction): $J_H^2 \chi c^\dagger_{\boldsymbol{r}\alpha} \sigma^a_{\alpha\beta} c_{\boldsymbol{r}\beta} c^\dagger_{\boldsymbol{r}+\hat{y},\alpha'} \sigma^a_{\alpha'\beta'} c_{\boldsymbol{r}+\hat{y},\beta'}$. This interaction results in a phase transition to a nematic state with order parameter $\langle c^\dagger_{\boldsymbol{r}+\hat{y},\alpha} c_{\boldsymbol{r},\alpha}\rangle \neq 0$, or more generally, $\varphi_c \equiv \langle c^\dagger_{\boldsymbol{r}+\hat{x},\alpha} c_{\boldsymbol{r},\alpha} - c^\dagger_{\boldsymbol{r}+\hat{y},\alpha} c_{\boldsymbol{r},\alpha}\rangle \neq 0$.

Furthermore, the induced interaction leads to pairing among the itinerant electrons. Since the spin fluctuations are antiferromagnetic, one expects pairing in the spin singlet channel. We then mean field decompose the induced interaction into spin singlet pairing channel with the corresponding pair operator $h^\dagger_{\alpha\alpha'}(\boldsymbol{k}) = \frac{1}{\sqrt{2}} \left(c^\dagger_{\boldsymbol{k}\alpha\uparrow} c^\dagger_{-\boldsymbol{k}\alpha'\downarrow} - c^\dagger_{\boldsymbol{k}\alpha\downarrow} c^\dagger_{-\boldsymbol{k}\alpha'\uparrow}\right)$. Due to the special form of spin susceptibility and band structure in FeSe, the pairing problem is largely simplified. The spin fluctuations enter the pairing problem through the spin susceptibility $\chi(\boldsymbol{q}) \equiv \chi(\boldsymbol{q}, \Omega_n = 0)$, which can be obtained from the dynamic spin structure factor via $\chi(\boldsymbol{q}) = -\int d\omega \mathcal{S}_{\boldsymbol{q},\omega}/\omega$. The special form of $\chi(\boldsymbol{q})$ in FeSe (see Fig. 9) results in only inter-band pairing correlation among the three Fermi pockets. Furthermore, since Hund's coupling is diagonal in orbital space, there are only pairing correlations between the same orbitals: in orbital basis, the pairing interaction is of the form $\mathcal{H}_{\rm pair} \sim J_\alpha^2 \chi(\boldsymbol{k} - \boldsymbol{k}') h^\dagger_{\alpha\alpha}(\boldsymbol{k}) h_{\alpha\alpha}(\boldsymbol{k}')$.

Pairing occurs near the Fermi surface, which is naturally expressed in the band basis. We then transform from the orbital basis to the band basis: $c^\dagger_{\boldsymbol{k}\alpha\mu} = \sum_a \eta^*_{\alpha a\mu}(\boldsymbol{k}) d^\dagger_{\boldsymbol{k}a\mu}$ with band index a. Note that since the spin-orbit

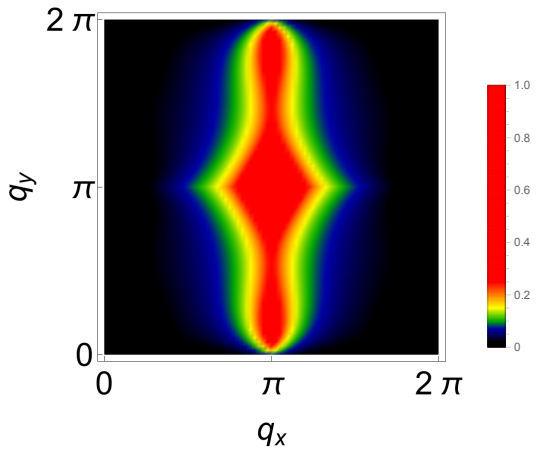

FIG. 9: (Color online) The spin susceptibility $\chi(\boldsymbol{q}) \equiv \chi(\boldsymbol{q}, \Omega_n = 0)$ in a single nematic domains.

coupling here is in the σ^3 channel, different spins do not mix. The pair operator in the band basis is $h_a^\dagger(\boldsymbol{k}) = \frac{1}{\sqrt{2}}\left(d^\dagger_{\boldsymbol{k}a\uparrow} d^\dagger_{-\boldsymbol{k}a\downarrow} - d^\dagger_{\boldsymbol{k}a\downarrow} d^\dagger_{-\boldsymbol{k}a\uparrow}\right)$. Omitting the frequency dependence, the pairing Hamiltonian is of the form

$$\mathcal{H}_{\text{pair}} = \sum_{\boldsymbol{k}\boldsymbol{k}'ab} \Gamma_{ab}(\boldsymbol{k}, \boldsymbol{k}') h_a^\dagger(\boldsymbol{k}) h_b(\boldsymbol{k}'), \tag{24}$$

with the projected pairing interaction $\Gamma_{ab}(\boldsymbol{k}, \boldsymbol{k}') = \frac{1}{2}\sum_\alpha J_\alpha^2 \chi(\boldsymbol{k} - \boldsymbol{k}') M^*_{\alpha a}(\boldsymbol{k}) M_{\alpha b}(\boldsymbol{k}')$. The orbital content is encoded in the form factor $M_{\alpha a}(\boldsymbol{k}) = \eta_{\alpha a\uparrow}(\boldsymbol{k})\eta_{\alpha a\downarrow}(-\boldsymbol{k})$. The gap function is then defined as $\Delta_a(\boldsymbol{k}) = \sum_{\boldsymbol{k}'b} \Gamma_{ab}(\boldsymbol{k}, \boldsymbol{k}')\langle h_b(\boldsymbol{k}')\rangle$. The gap symmetry function $g_i(\boldsymbol{k}) \propto \Delta_a(\boldsymbol{k})$ on the Fermi surface is determined by the eigen equation

$$-\sum_j \oint_{\text{FS}_j} \frac{d\boldsymbol{k}'_\parallel}{2\pi v_F(\boldsymbol{k}')} \Gamma_{ij}(\boldsymbol{k}, \boldsymbol{k}') g_j(\boldsymbol{k}') = \lambda g_i(\boldsymbol{k}), \tag{25}$$

where $\boldsymbol{k}_\parallel$ denotes momentum along the Fermi surface FS_j, and $v_F(\boldsymbol{k}) = |\nabla E_a(\boldsymbol{k})|$ represents the Fermi velocity. We can then solve the above eigen equation to find the leading eigenvalue and the corresponding eigenvector, which determines the resulting gap structure within a single nematic domain. The inputs are (1) itinerant electron band structure encoded in $\epsilon^{\mu\nu}_{\alpha\beta}(\boldsymbol{k})$ (2) local moment spin susceptibility $\chi(\boldsymbol{q})$, and (3) Hund's couplings J_α.

We show here more concretely how (π, π) spin fluctuation mediated pairing enhances the superconducting T_c. We first estimate the value of λ in bulk FeSe from the observed T_c. Since Fermi energy is small compared to spin fluctuation scale (so called antiadiabatic limit), Fermi energy acts as cutoff in the T_c equation: $T_c \sim E_F e^{-1/\lambda}$.[61,62] With $T_c \sim 8$ K, $E_F \sim 10$ meV,[63] we obtain $\lambda \sim 0.37$. In bulk FeSe, pairing occurs predominantly among d_{yz} orbitals as mediated by $(\pi, 0)$ spin fluctuations, while (π, π) spin fluctuation mediated pairing among d_{xy} orbitals is largely suppressed. This corresponds to taking $(J_{xy}, J_{zx}, J_{yz}) \sim (0, 1, 1)$. (Note that due to the near absence of $(0, \pi)$ spin fluctuations, pairing among d_{zx} orbitals is suppressed for any coupling. So we just set $J_{zx} = 1$.) When pairing is predominantly among d_{xy} orbitals, we have $(J_{xy}, J_{zx}, J_{yz}) \sim (1, 1, 0)$. We have obtained the resulting eigenvalue $\lambda' = 2.98\lambda$, which gives $T_c \sim 47$ K. Hence (π, π) spin fluctuation mediated pairing is indeed able to account for the much higher T_c in heavily doped FeSe ($T_c \sim 48$ K),[64] and a large part of the T_c increase in monolayer FeSe ($T_c \sim 50 - 64$ K).[65]